Soft Matter

PAPER

View Article Online
View Journal | View Issue

Check for updates

Cite this: *Soft Matter*, 2018, **14**, 4852

Dissipative assemblies that inhibit their deactivation†

Benedikt Rieß,‡[a] Caren Wanzke,‡[a] Marta Tena-Solsona,[ab] Raphael K. Grötsch,[a] Chandan Maity[a] and Job Boekhoven *[ab]

Received 20th April 2018,
Accepted 22nd May 2018

DOI: 10.1039/c8sm00822a

rsc.li/soft-matter-journal

Dissipative self-assembly is a process in which energy-consuming chemical reaction networks drive the assembly of molecules. Prominent examples from biology include the GTP-fueled microtubule and ATP-driven actin assembly. Pattern formation and oscillatory behavior are some of the unique properties of the emerging assemblies. While artificial counterparts exist, researchers have not observed such complex responses. One reason for the missing complexity is the lack of feedback mechanisms of the assemblies on their chemical reaction network. In this work, we describe the dissipative self-assembly of colloids that protect the hydrolysis of their building blocks. The mechanism of inhibition is generalized and explored for other building blocks. We show that we can tune the level of inhibition by the assemblies. Finally, we show that the robustness of the assemblies towards starvation is affected by the degree of inhibition.

Published on 23 May 2018. Downloaded by Technical University of Munich on 14/06/2018 07:24:31.

Introduction

Molecular self-assembly into various structures has received widespread attention over the past decades[1–5] and has resulted in biomaterials,[6,7] catalysts,[8] molecular electronics,[9] and many other supramolecular materials.[10] Inspired by biological assemblies such as the GTP-driven assembly of microtubules,[11] or the ATP-fueled crosslinking of actin filaments,[12] the dissipative self-assembly of non-biological molecules has been pioneered.[13] In dissipative assembly, the assembly process is induced by a chemical reaction network that consists of at least two chemical reactions.[14–18] First, a precursor is activated for self-assembly by the irreversible consumption of a high-energy molecule (fuel) or photon (light). We refer to this reaction as the activation reaction. A second reaction reverts the activated product spontaneously to its initial precursor state. We refer to this reaction as the deactivation. The activated product, in its limited lifetime, can self-assemble. Researchers have described both light-driven[19] and fuel-driven[13,20] dissipative assembly.

The kinetics of the activation and deactivation control the material properties of dissipative assemblies, which makes them intrinsically different than their in-equilibrium counterparts. For example, these materials can be controlled over space and time which opens the door to temporary materials with a predefined lifetime. To that end, researchers have developed self-erasing inks,[21,22] hydrogels that disappear after a predefined lifetime[22–25] colloids that can release hydrophobic molecules after a tunable time,[22] and others.[26–29] Other unique material properties of dissipative assemblies, include adaptivity and autonomous self-healing.[23]

Until now, the complex behavior we find in dissipative biological assemblies, like oscillations or pattern formation,[30] have not been observed in artificial analogs. A reason for the discrepancy in complex behavior in dissipative assemblies is the lack of feedback mechanisms of dissipative assemblies on their chemical reaction network. For example, the assembly of tubulin into microtubules catalyzes its own deactivation.[31] One of the goals for the field of dissipative self-assembly is thus to implement mechanisms by which the assemblies exert feedback on their activation and deactivation reaction.

We recently introduced a new chemical reaction network that takes place in buffered water at pH 6.[22] The chemical reaction network converts a dicarboxylate precursor into a transient anhydride at the expense of a carbodiimide (Scheme 1a). In the activation reaction, derivatives of aspartic (D) or glutamic (E) acid reacted with a carbodiimide to form their corresponding *O*-acylisourea. This *O*-acylisourea further reacted to form its corresponding anhydride. The reaction released one molecule of urea. We called the urea waste, as it had no further function in the cycle. Our previous study has shown that the waste does not affect the assemblies or kinetics significantly.[22] In the deactivation reaction, the anhydride hydrolyzed back to the original dicarboxylate precursor. Upon addition of a finite amount of

[a] *Department of Chemistry, Technical University of Munich, Lichtenbergstrasse 4, 85748 Garching, Germany. E-mail: job.boekhoven@tum.de*
[b] *Institute for Advanced Study, Technical University of Munich, Lichtenbergstrasse 2a, 85748 Garching, Germany*

† Electronic supplementary information (ESI) available. See DOI: 10.1039/c8sm00822a

‡ These authors contributed equally to this work.

This journal is © The Royal Society of Chemistry 2018

Published on 23 May 2018. Downloaded by Technical University of Munich on 14/06/2018 07:24:31.

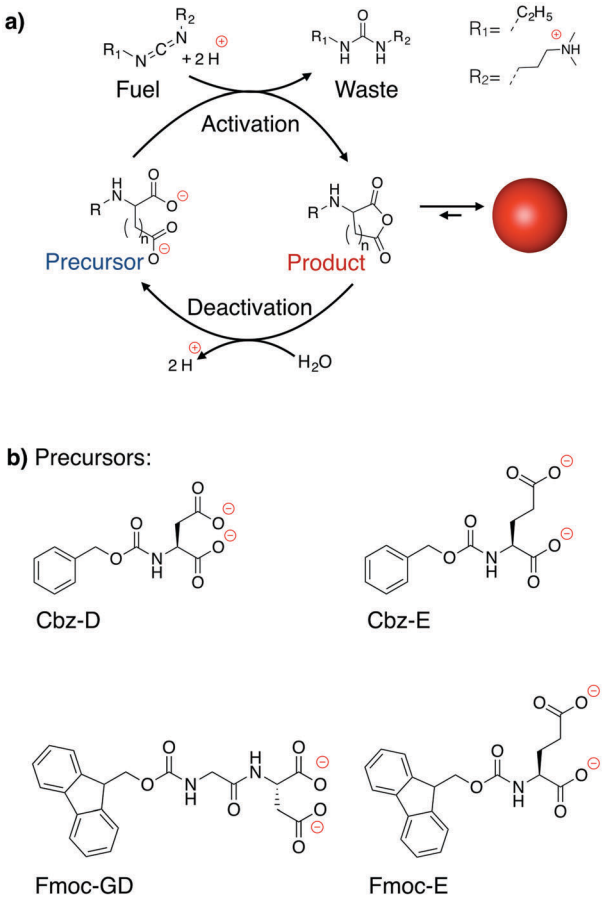

Scheme 1 (a) The chemical reaction network employed to drive self-assembly of anhydrides. The dicarboxylate precursor is converted into the metastable product (anhydride) by a high energy condensing agent (EDC). For Fmoc-E or Fmoc-GD as a precursor, this product is able to self-assemble into colloids. In the aqueous environment, the product is hydrolyzed back to the precursor. (b) The molecular structure of precursors used in this study.

carbodiimide fuel, the anhydride was temporarily present at the expense of the carbodiimide. Work by others demonstrated the generality of the carbodiimide induced transient anhydride formation.[32]

While the dicarboxylate precursor carried two anions, the anhydride was charge-neutral. This hydrophobization converted soluble precursors into assembling anhydride products. We found that one specific precursor, *N*-fluorenylmethyloxycarbonyl glutamic acid (Fmoc-E), formed colloids. These colloids significantly decreased the rate of hydrolysis of its anhydride building blocks.

In the current work, we study the underlying mechanism of the inhibition of the hydrolysis reaction in the presence of colloids. We show that the mechanism is a result of the assemblies protecting its anhydride product from deactivation and that the mechanism can be generalized for other colloid-forming anhydrides. We demonstrate that we can tune the level of the inhibition of the hydrolysis. With that control, we can manipulate the survival time of the colloids and their robustness towards periods of starvation from their energy source.

Results and discussion

Chemical reaction network

We studied the kinetics of the chemical reaction network using four different dicarboxylate precursors (Scheme 1b). Two precursors were derivatives of aspartic acid (D), while the other two were derivatives of glutamic acid (E). Of the aspartic acid derivatives, we used the *N*-carboxybenzyl protected amino acid (Cbz-D), and an *N*-fluorenylmethyloxycarbonyl protected-glycine derivative (Fmoc-GD). Of the glutamic acid derivatives, we investigated Cbz-E and Fmoc-E. The anhydrides of the Cbz-amino acids were well soluble under all experimental conditions, whereas the anhydrides of Fmoc-E and Fmoc-GD assembled into colloids (*vide infra*). In all experiments, we used 10 mM solutions of the precursor in water buffered at pH 6 with MES. We added finite amounts of carbodiimide as fuel (1-ethyl-3-(3-dimethylaminopropyl)carbodiimide, EDC) to these solutions and measured the response of the chemical reaction network by high-pressure liquid chromatography and electrospray ionization mass spectroscopy (HPLC, ESI-MS, Fig. 1 and Tables S1–S3, ESI†). It should be noted that the reactions between fuel and Fmoc-E or Cbz-E resulted in a small amount of the *N*-acylurea (Table S3, ESI†) which did not interfere with the other reactions or the assemblies. Finally, we should note that our HPLC method was optimized and verified to ensure that all anhydride, be it in an assembly or not, was injected. In other words, the assembling species was not filtered out by the analysis method neither did it sediment during the experiment.

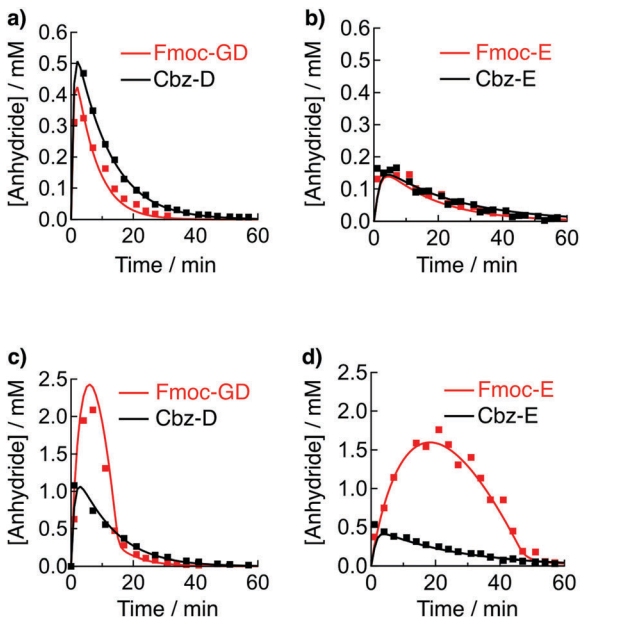

Fig. 1 Concentration anhydride against time in response to addition of EDC as determined by HPLC (markers) or the kinetic model (solid line) for (a) 10 mM Fmoc-GD (red) or Cbz-D (black) with 10 mM EDC, (b) 10 mM Fmoc-E (red) or Cbz-E (black) with 3 mM EDC, (c) 10 mM Fmoc-GD (red) or Cbz-D (black) with 25 mM EDC, (d) 10 mM Fmoc-E (red) and Cbz-E (black) with 10 mM EDC.

Published on 23 May 2018. Downloaded by Technical University of Munich on 14/06/2018 07:24:31.

We recorded the concentration of the fuel, the precursor, and the product over time (Fig. 1a and b). These concentrations were used to fit a previously described kinetic model.[22] The model could be used to predict the concentrations accurately when the chemical reaction network did not produce any assemblies (Fig. 1a and b, the rate constants can be found in Table S4, see Supplementary Notes 1 for a description of the kinetic model, ESI†). We found similar yields, reaction times and *k*-values for precursors based on the same terminal amino acid demonstrating that the reactivity was not drastically affected by the protecting group. For example, adding 3 mM of EDC to Cbz-E or Fmoc-E resulted in a maximum concentration of anhydride of 0.15 mM after 5 minutes.

When we added relatively large batches of fuel, differences between the evolution of the concentration product of Cbz-D and Fmoc-GD, as well as Cbz-E and Fmoc-E were evident (Fig. 1c and d). For instance, when we added 10 mM of EDC to 10 mM of Cbz-E, a maximum concentration of anhydride was found after 5 minutes at 0.42 mM whereas, for the same experiment with Fmoc-E, the maximum anhydride was a four-fold higher at 1.6 mM after 18 minutes. Similar higher anhydride concentrations and delays of the maxima were found for Fmoc-GD when compared to Cbz-D. The apparent change in the kinetics was not a result of a change in the activation kinetics as the EDC consumption showed a similar profile for Cbz-E compared to Fmoc-E as well as Cbz-D compared to Fmoc-GD (Fig. S1a and b, ESI†).

Morphological assessment of the assemblies

We used dynamic light scattering (DLS) to assess the nature of the assemblies of the anhydrides of Fmoc-E and Fmoc-GD. We initiated the cycle by addition of 10 mM EDC to 10 mM Fmoc-E, or 25 mM EDC to 10 mM Fmoc-GD which rapidly turned the transparent precursor solutions turbid. We measured an increase in the DLS scattering rate of at least an order of magnitude compared to before addition of fuel for both Fmoc-GD and Fmoc-E (Fig. 2a and b). The radii calculated by the fitted DLS data peaked after roughly 7 minutes at 390 nm, and after 20 minutes at 550 nm for Fmoc-GD and Fmoc-E, respectively (Fig. 2c and d). It is worth to note that these times correspond to the time of maximum anhydride concentration. The increased turbidity was temporary, and the scattering rates decreased to their original values after roughly 15 and 50 minutes, respectively. We found no evidence for assemblies when adding 10 mM or 3 mM of EDC to Fmoc-GD or Fmoc-E, respectively (Fig. 2a and b).

We utilized fluorescence microscopy with Nile Red as a hydrophobic dye to further assess the assemblies. Microscopy showed no assemblies before addition of the fuel. In contrast, minutes after addition of fuel, colloids were found for both Fmoc-GD and Fmoc-E (Fig. 3a–d). Using image analysis software on micrographs taken around 7 minutes for Fmoc-GD and 20 minutes for Fmoc-E, the radii of at least 2500 colloids were measured. The radii of the colloids were found to be in line with those found by DLS: 0.35 μm for Fmoc-GD and 0.4 μm for Fmoc-E (Fig. 3e and f). Finally, cryo-TEM microscopy further confirmed

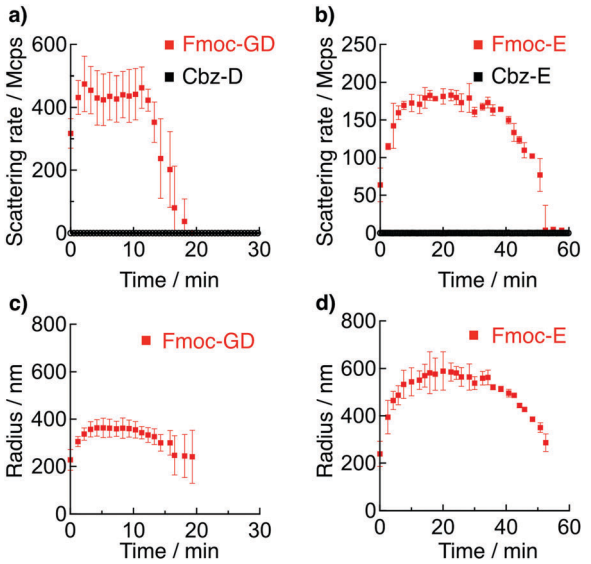

Fig. 2 Scattering rates against time as measured by DLS (a) Fmoc-GD (red) or Cbz-D (black) and 25 mM EDC, and (b) Fmoc-E (red) or Cbz-E (black) with 10 mM EDC. Note that the Cbz-based experiments did not increase the turbidity and their scattering rate thus remains around 0. (c and d) Hydrodynamic radii against time for the experiments described in a and b, respectively. We obtained no reliable data for the Cbz-based precursors because of the limited scattering. All error bars represent the standard deviation of the mean for a sample size $n = 3$.

that the colloids were already present within the first minutes of the chemical reaction network with a radius in the range of 300 to 400 nm (Fig. 3g and h). From all of the above observations, we concluded that the increased anhydride concentrations were a result of the presence of the colloids.

Mechanism of inhibition of the deactivation

In the following, we explain the mechanism of inhibition. In the presence of colloids, the activation of the anhydride remained unchanged (Fig. S1a and b, ESI†). The difference in the kinetics in the presence of colloids must thus be a result of the deactivation reaction. To that end, we hypothesized that the assemblies protect the anhydride from hydrolysis, *via* a simple mechanism. The colloids are relatively large and hydrophobic, which means that any anhydride in these colloids is effectively separated from the aqueous environment. In other words, the colloids protect their anhydrides from hydrolysis, but only the fraction that is found in the colloids. The anhydride that remained in solution thus remained susceptible to hydrolysis. The protection from hydrolysis explained the relatively high concentration of anhydride when colloids were formed.

To confirm our hypothesis, we adjusted the kinetic model to exclude from hydrolysis the fraction of the anhydride above the critical aggregation concentration (CAC). In other words, hydrolysis of the anhydride only occurred on the fraction that remained in solution, and hydrolysis was thus limited to a rate of $v_4 = k_4 \times \mathrm{CAC}$. In that equation, k_4 is the first order rate constant for hydrolysis in solution. Empirically determining the CAC was challenging, given the metastability of the anhydride.

 This journal is © The Royal Society of Chemistry 2018

Published on 23 May 2018. Downloaded by Technical University of Munich on 14/06/2018 07:24:31.

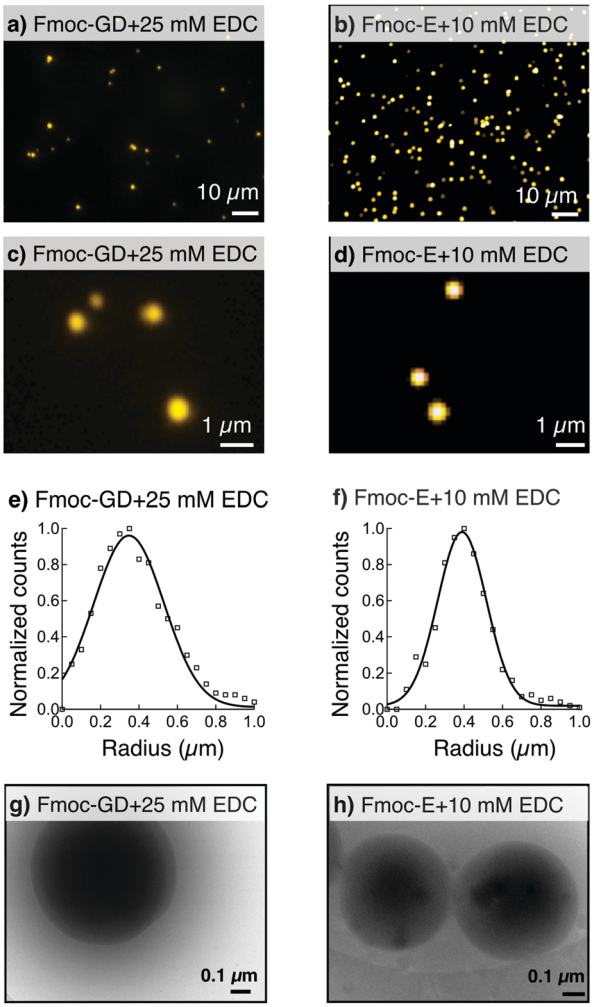

Fig. 3 Fluorescence microscopy micrographs of (a) Fmoc-GD with 25 mM EDC after roughly 7 minutes and (b) Fmoc-E with 10 mM EDC after roughly 20 minutes. Fluorescence microscopy micrographs of (c) Fmoc-GD with 25 mM EDC after roughly 7 minutes and (d) Fmoc-E with 10 mM EDC after roughly 20 minutes, with high magnification. (e and f) Histograms of the normalized colloid's radii distribution ($n > 2500$) of the micrographs of (c) and (d), respectively. Cryo-TEM of colloids under the same conditions in the first minute for (g) Fmoc-E and (h) Fmoc-GD.

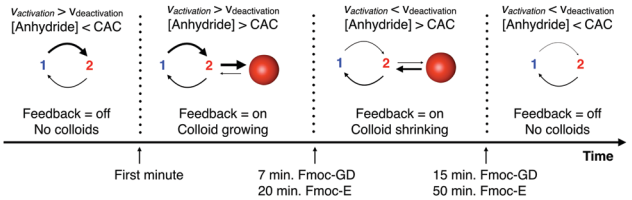

Fig. 4 Mechanism of kinetically controlled assembly into colloids during a dissipative cycle. The assemblies inhibit deactivation of anhydride (**2**) to carboxylate (**1**).

Instead, we used the updated kinetic model and adjusted the CAC to fit the HPLC data (Table S4, ESI†). Since both k_4 and the CAC are both constants, the resulting rate is also a constant, *i.e.*, the hydrolysis followed 0th order kinetics. This rather simple addition to the kinetic model allowed us to fit all HPLC data for cycles that did or did not form assemblies (Fig. 1a–d).

Fig. 4 depicts a tentative mechanism of the evolution of the dissipative cycle. At the beginning of the cycle, the rate of building block activation was high, because the amount of fuel was at its highest. Within the first minute, the solution reached supersaturation and excess anhydride self-assembled into colloids. When these first colloids were present, we hypothesized that any activated anhydride was deposited on the existing colloids. This deposition was confirmed by the increase in radius as observed by DLS (Fig. 2). After 7 minutes for Fmoc-GD and 20 minutes for Fmoc-E, the fuel level had decreased such that the activation rate is lower than hydrolysis rate. The net anhydride formation was thus negative, and the concentration of anhydride in the system decreased. As the hydrolysis happened in solution, the solution became undersaturated. The undersaturated solution could now accept anhydride from the colloids, resulting in a decrease of the colloids radii. Here, we assumed that anhydride disassembly from the colloids is faster than hydrolysis.[33] The colloids kept on supplying the undersaturated solution with anhydride until they had disappeared. At this point, the inhibition is switched off, and hydrolysis proceeded with first order kinetics.

While we understood the above mechanism qualitatively for Fmoc-E, we confirmed the mechanism for other colloid-forming assemblies and could quantitatively express the level of inhibition with our kinetic model. The quantitative understanding allows us to set some preliminary design rules for this type of inhibition in dissipative assemblies. First, the deactivation reaction of the assembling species needs to be driven either by reaction with the solvent or a reagent in the solvent. The assembly needs to be sufficiently large compared to its building blocks in all three dimensions, and it needs to exclude the building blocks from the solvent. We mention large in three dimensions, as we have not seen this effect in large one-dimensional fibers.[22] Under these conditions, the assemblies protected their anhydride building blocks from hydrolysis. Finally, the disassembly rate is required to be faster than the hydrolysis rate, such that the rate determining step is the hydrolysis and not the exchange of building blocks between assemblies and solution.

Tuning the deactivation inhibition

We wondered if we could control the level of inhibition of the assemblies on the anhydride hydrolysis rate. We first performed experiments under conditions that prevent the self-assembly of the anhydride of Fmoc-E into the observed colloids. To do so, we added 1.0 mM of cetyltrimethylammonium bromide[34] (CTAB). CTAB is a common cationic surfactant with a critical micelle concentration of 0.1 mM under the employed conditions (Fig. S2, ESI†). We reasoned that CTAB micelles would solubilize the anhydride of Fmoc-E, thus inhibiting its self-assembly into colloids. Indeed, with CTAB, no increased turbidity was found after addition of 10 mM EDC to 10 mM Fmoc-E. HPLC analysis showed that the EDC consumption rate was similar compared to without CTAB (Fig. S1c, ESI†). However, the

Published on 23 May 2018. Downloaded by Technical University of Munich on 14/06/2018 07:24:31.

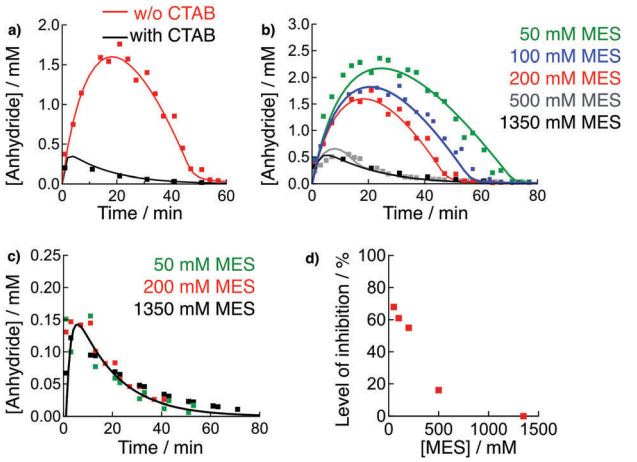

Fig. 5 (a) The concentration of Fmoc-E anhydride in response to 10 mM EDC with (black) or without (red) 1 mM of CTAB. (b) The concentration of Fmoc-E anhydride in response to 10 mM EDC with varying MES concentration. (c) The same experiment at b, but with only 3 mM of EDC. (d) Level of inhibition against the concentration of MES buffer. The inhibition level scaled between 0 and 100% where 0% is no inhibition, and 100% is complete inhibition of the hydrolysis.

anhydride concentration remained much lower compared to without CTAB (Fig. 5a). The HPLC data was fitted using the kinetic model, and we obtained a good fit by removing the inhibition mechanism (Table S4, ESI†). In summary, the addition of the surfactant increased the anhydride solubility and prevented the formation of colloids required for the inhibition of the deactivation.

In the next experiments, we aimed at tuning the level of inhibition by the colloids. To do so, the CAC is to be altered by minimal amounts. We found that the concentration MES buffer could tune the solubility of the precursor, *i.e.*, the more MES we added, the higher the solubility (Fig. S3, ESI†). Such an effect is referred to as "salting in."[35] We assumed a similar trend for the anhydride of Fmoc-E. We also verified that at the relatively low buffer concentration of 50 mM MES, the buffer still had sufficient capacity to diminish fluctuations in pH (Fig. S4, ESI†). Addition of 10 mM EDC to 10 mM Fmoc-E in 50 mM MES buffer at pH 6 resulted in a maximum anhydride concentration around 2.5 mM (Fig. 5b). In contrast, when we performed the same experiment in 1350 mM MES, the maximum anhydride concentration was only 0.5 mM, and the evolution of the anhydride concentration resembled the one without the inhibition mechanism. To our surprise, the drastically different evolution of the chemical reaction network could be fitted by only adjusting the CAC in the kinetic model (Fig. 5b). The CAC in 200 mM MES was previously fitted to be 0.24 mM. For 50 mM MES, a good fit was obtained by decreasing the CAC to 0.17 mM. In contrast, for 1350 mM, we removed the inhibition mechanism to obtain a good fit (Fig. 5b).

As a control, we carried out a similar experiment but added only 3 mM of EDC to ensure the absence of assemblies under any of the conditions. Under these control conditions, the evolution of the anhydride concentration was similar for each buffer concentration (Fig. 5c). We quantified the level of inhibition by calculating the 0th order hydrolysis rate as a fraction of the maximum hydrolysis rate without inhibition (Fig. 5d and Supplementary Notes 2, ESI† for calculations). In this calculation, 0% equals no inhibition, and 100% implies a complete inhibition of the hydrolysis.

Inhibition of deactivation makes the assemblies more robust

Finally, we set out to test the robustness of our assemblies towards periods of starvation. We fueled our assemblies with a batch of 10 mM EDC. After the fueling, we starved them from fuel for 50 minutes after which we gave them another batch of 10 mM EDC. We performed this fueling-starvation sequence for three rounds. We tested the response of two levels of inhibition: a system with an intermediate amount of inhibition (±50% at 200 mM MES) and a system with a high amount of inhibition (±70% at 50 mM MES). The model showed that for a low amount of inhibition, the concentration anhydride would fall below the CAC in the starvation period (Fig. 6a). In contrast, in the high inhibition experiment, the concentration would remain above the CAC throughout the experiment. In other words, in the high inhibition experiments, colloids can "survive" the entire experiment, whereas a colloid in the intermediate inhibition experiment will likely disassemble.

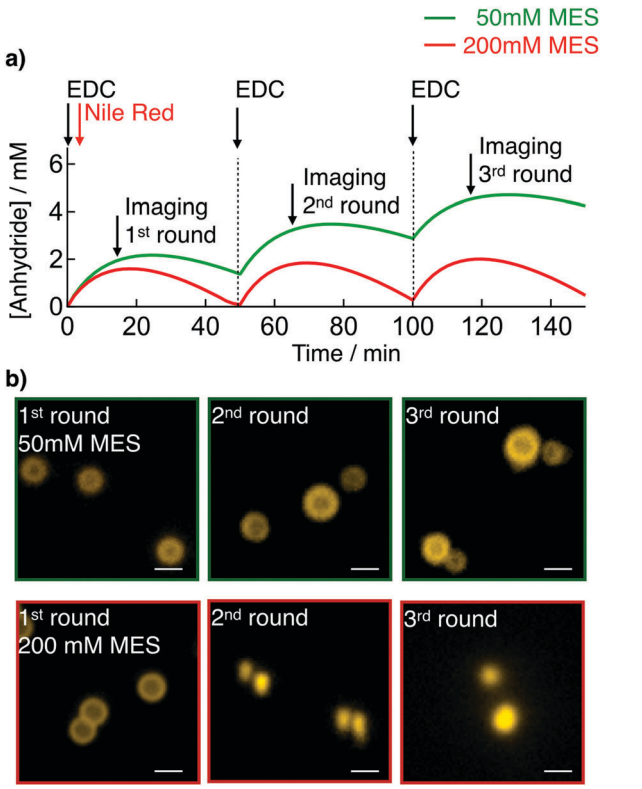

Fig. 6 (a) The concentration of anhydride against time as calculated by the kinetic model. Every 50 minutes a new batch of 10 mM EDC is added. 15 minutes after addition of EDC the solutions were imaged. (b) Micrographs of the samples as described in Fig. 4d. Scale bar corresponds to 1 μm. The left micrographs correspond to 50 mM MES and the right ones to 200 mM MES.

This journal is © The Royal Society of Chemistry 2018

Published on 23 May 2018. Downloaded by Technical University of Munich on 14/06/2018 07:24:31.

To confirm the survival or disassembly of the colloids, we had to mark them with a dye that could distinguish colloids that had disassembled from colloids that had remained assembled. To do so, 5 minutes after initiating the first cycle, 2.5 μM Nile Red was added. In the first 5 minutes, the colloids had grown to roughly 400 nm in radius. That means that the hydrophobic dye could only incorporate into a layer around the core of the particles, which looked like a ring under the microscope (Fig. 6b). If the colloids disassembled and reassembled later, they lost that unique dye distribution, which allowed us to distinguish them from colloids that had survived the experiment (*vide infra*). The samples were imaged 20 minutes after each fuel addition. In the first fueling round, microscopy revealed colloids of roughly 1 μm with the characteristic ring (Fig. 6b). After the 50 minute-starvation period, the second batch of fuel was added. In the second fueling round, both solutions showed particles of roughly 1 μm. In the high inhibition-experiment, microscopy showed particles, that maintained the characteristic ring, serving as a strong indication that they had survived the starvation period. In contrast, the colloids with intermediate inhibition showed a homogeneous distribution of the dye through the core of the particle (Fig. 6b). After the second starvation period, the system was refueled for the third time. The final imaging round showed similar particles as the second round.

The layered dye distribution throughout the colloids rendered them unique, and only a colloid that "survived" the entire experiment could carry the unique color code. In contrast, a particle that had disassembled would have released its dye into the solution and subsequently reincorporated it into the core of new colloids upon addition of new fuel. The coding allowed us to discriminate particles that had "survived" the starvation from particles that had "died." These last experiments show that our colloids with a high level of inhibition all "survived" the starvation periods of 50 minutes. In contrast, the particles with low inhibition did not show the color coding and had thus fully disassembled during the starvation period.

Conclusions

Our work shows a method of incorporating a feedback mechanism into dissipative non-equilibrium assemblies. The understanding of the molecular mechanisms at play allows us to switch on or off the inhibition or to tune it. We show that increasing inhibition gives the inherently unstable assemblies increased robustness towards starvation periods.

Experimental

Materials

Fmoc-E, Cbz-E, Cbz-D, EDC, urea, MES were purchased from Sigma-Aldrich and Alfa-Aesar and used without any further purification unless otherwise indicated. Fmoc-GD was synthesized using standard fluoren-9-ylmethoxycarbonyl (Fmoc) solid-phase peptide synthesis on Wang resin (100–200 mesh, 1.1 mmol g^{-1} loading). Peptides were synthesized on a CEM Liberty microwave-assisted peptide synthesizer. The ESI† gives a detailed description of the synthesis.

Kinetic model. We used a kinetic model to predict the evolution of the anhydride concentration over time. In brief, the kinetic model uses rate constant for six reactions in the chemical reaction network. Each second, the kinetic model calculates the concentrations of the reactants and product. The kinetic model and MatLab code are described in detail Supplementary Notes 1 (ESI†). Table S4 (ESI†) gives the rate constants.

Dynamic light scattering. We carried out DLS measurements on all solutions with a DynaPro NanoStar from Wyatt with a laser wavelength of 658 nm in disposable cuvette for DLS from Wyatt. The measurements for Fmoc-E with 10 mM EDC and Fmoc-GD with 25 mM EDC consisted of 5 acquisitions with an acquisition time of 10 seconds. The remaining experiments consisted of 1 acquisition with an acquisition time of 5 seconds. For measurements and analysis, we used the software Dynamics V7.

HPLC. We monitored the kinetics of the chemical reaction networks over time by using analytical HPLC (HPLC, Thermofisher Dionex Ultimate 3000, Hypersil Gold 250 × 4.8 mm). A 750 μL sample was prepared as described above and placed into a screw cap HPLC vial. We injected samples of the solutions directly, without further dilution. The HPLC separated all compounds involved using a linear gradient of water with 0.1% TFA : ACN with 0.1% TFA from 40 : 60 to 2 : 98.

We performed calibration curves for the EDC (λ_{abs} = 220 nm) and precursors (λ_{abs} = 254 nm) in triplicate. Calibration was not possible for the anhydrides due to their intrinsic instability. Instead, we used the absorption coefficient of their corresponding precursor.

Fluorescence microscopy. Fluorescence microscopy was performed on a Leica DMi8 microscope using a 63× oil immersion objective. We prepared samples as described above but with 25 μM Nile Red as a dye. We deposited 20 μL of the sample on the glass slide and covered with a 12 mm diameter coverslip. Samples were excited with 543 nm laser and imaged at 580–700 nm. Particle diameters were counted using ImageJ cell counting package.

ESI. ESI-MS measurements were performed using a Varian 500 MS LC ion trap spectrometer. The samples were diluted in acetonitrile and injected into an acetonitrile carrier flow (20 μL min^{-1}).

Cryogenic-transmission electron microscopy (cryo-TEM). Samples for TEM were prepared as described above. The grids (Quantifoil R2/2 on Cu-grid 400 mesh) were freshly glow-discharged for 30 (Fmoc-GD) or 90 seconds (Fmoc-E) before use. Preparation of the grids was performed in an FEI/Thermo Fisher Vitrobot at 25 °C with the relative humidity set to 100%. Fmoc-GD (5 μL) was incubated for 30 seconds, blotted twice for 3.5 seconds (blotting force set to −5) and then directly plunged into liquid ethane that was pre-cooled by liquid nitrogen. Fmoc-E (5 μL) was incubated for 15 seconds, blotted for 2 seconds (blotting force set to −1) and then also directly plunged into liquid ethane.

Published on 23 May 2018. Downloaded by Technical University of Munich on 14/06/2018 07:24:31.

The cryo-EM grids were transferred and stored in liquid nitrogen, and when needed, placed into a Gatan cryo-transfer-specimen holder to insert into the microscope. The specimen temperature was maintained at −170 °C during the data collection. Cryo-TEM imaging of Fmoc-GD was performed on a Jeol JEM-1400 plus operating at 120 kV, and Cryo-TEM imaging of Fmoc-E was performed on a Tecnai Spirit microscope (FEI/Thermo Fisher) operating at 120 kV. The images were recorded in a low-dose mode on a CCD camera.

Solubility determination of precursors. The samples of Fmoc-E (10 mM) were prepared as described above in different buffer concentrations (50, 100, 200, 500 and 1350 mM MES). After the pH was adjusted to 1, the precipitate was filtered off with a 200 nm syringe filter. HPLC analysis was carried out like described above to determine the remaining Fmoc-E in solution.

Sample preparation. Stock solutions of the precursor were prepared by dissolving the precursor in MES buffer, after which the pH was adjusted to pH 6.0. Stock solutions of EDC were prepared by dissolving the EDC powder in MQ water. Typically, stock solutions of 1.0 M EDC were used freshly. Reaction networks were started by addition of the high concentration EDC to the peptide solution. All analysis was carried out at 25 °C.

Conflicts of interest

There are no conflicts to declare.

Acknowledgements

J. B. is grateful for funding by the Technical University of Munich – Institute for Advanced Study, funded by the German Excellence Initiative and the European Union Seventh Framework Programme under grant agreement no. 291763. B. R. acknowledges the Deutsche Forschungsgemeinschaft within the SFB No. 863. R. G. is grateful for funding by the International Research Training Group ATUMS (IRTG 2022). M. T. S. acknowledges the European Union's Horizon 2020 Research and Innovation program for the Marie Sklodowska Curie Fellowship under grant agreement no. 747007.

References

1 J. D. Hartgerink, E. Beniash and S. I. Stupp, *Science*, 2001, **294**, 1684–1688.
2 J. P. Hill, W. Jin, A. Kosaka, T. Fukushima, H. Ichihara, T. Shimomura, K. Ito, T. Hashizume, N. Ishii and T. Aida, *Science*, 2004, **304**, 1481–1483.
3 P. A. Korevaar, S. J. George, A. J. Markvoort, M. M. Smulders, P. A. Hilbers, A. P. Schenning, T. F. De Greef and E. W. Meijer, *Nature*, 2012, **481**, 492–496.
4 A. Lampel, S. A. McPhee, H. A. Park, G. G. Scott, S. Humagain, D. R. Hekstra, B. Yoo, P. W. J. M. Frederix, T. D. Li, R. R. Abzalimov, S. G. Greenbaum, T. Tuttle, C. Hu, C. J. Bettinger and R. V. Ulijn, *Science*, 2017, **356**, 1064–1068.
5 P. W. Rothemund, *Nature*, 2006, **440**, 297–302.
6 G. A. Silva, C. Czeisler, K. L. Niece, E. Beniash, D. A. Harrington, J. A. Kessler and S. I. Stupp, *Science*, 2004, **303**, 1352–1355.
7 F. Tantakitti, J. Boekhoven, X. Wang, R. V. Kazantsev, T. Yu, J. Li, E. Zhuang, R. Zandi, J. H. Ortony, C. J. Newcomb, L. C. Palmer, G. S. Shekhawat, M. O. de la Cruz, G. C. Schatz and S. I. Stupp, *Nat. Mater.*, 2016, **15**, 469.
8 M. D. Pluth, R. G. Bergman and K. N. Raymond, *Science*, 2007, **316**, 85–88.
9 Y. Yamamoto, T. Fukushima, Y. Suna, N. Ishii, A. Saeki, S. Seki, S. Tagawa, M. Taniguchi, T. Kawai and T. Aida, *Science*, 2006, **314**, 1761–1764.
10 J. Boekhoven and S. I. Stupp, *Adv. Mater.*, 2014, **26**, 1642–1659; D. B. Amabilino, D. K. Smith and J. W. Steed, *Chem. Soc. Rev.*, 2017, **46**, 2404–2420.
11 A. Desai and T. J. Mitchison, *Annu. Rev. Cell Dev. Biol.*, 1997, **13**, 83–117.
12 S. Köhler, V. Schaller and A. R. Bausch, *Nat. Mater.*, 2011, **10**, 462–468.
13 J. Boekhoven, A. M. Brizard, K. N. Kowlgi, G. J. Koper, R. Eelkema and J. H. van Esch, *Angew. Chem., Int. Ed.*, 2010, **49**, 4825.
14 S. A. P. van Rossum, M. Tena-Solsona, J. H. van Esch, R. Eelkema and J. Boekhoven, *Chem. Soc. Rev.*, 2017, **46**, 5519–5535.
15 A. Sorrenti, J. Leira-Iglesias, A. J. Markvoort, T. F. de Greef and T. M. Hermans, *Chem. Soc. Rev.*, 2017, **46**, 5476–5490.
16 L. Heinen and A. Walther, *Soft Matter*, 2015, **11**, 7857–7866.
17 F. Della Sala, S. Neri, S. Maiti, J. L. Chen and L. J. Prins, *Curr. Opin. Biotechnol.*, 2017, **46**, 27–33.
18 R. Merindol and A. Walther, *Chem. Soc. Rev.*, 2017, **46**, 5588–5619.
19 J. J. de Jong, P. R. Hania, A. Pugzlys, L. N. Lucas, M. de Loos, R. M. Kellogg, B. L. Feringa, K. Duppen and J. H. van Esch, *Angew. Chem., Int. Ed.*, 2005, **44**, 2373–2376.
20 C. G. Pappas, I. R. Sasselli and R. V. Ulijn, *Angew. Chem., Int. Ed.*, 2015, **54**, 8119–8123.
21 R. Klajn, P. J. Wesson, K. J. Bishop and B. A. Grzybowski, *Angew. Chem., Int. Ed.*, 2009, **48**, 7035–7039.
22 M. Tena-Solsona, B. Rieß, R. K. Grötsch, F. C. Löhrer, C. Wanzke, B. Käsdorf, A. R. Bausch, P. Müller-Buschbaum, O. Lieleg and J. Boekhoven, *Nat. Commun.*, 2017, **8**, 15895.
23 T. Heuser, A.-K. Steppert, C. Molano Lopez, B. Zhu and A. Walther, *Nano Lett.*, 2014, **15**, 2213–2219.
24 C. G. Pappas, I. R. Sasselli and R. V. Ulijn, *Angew. Chem., Int. Ed.*, 2015, **54**, 8119–8123.
25 J. Boekhoven, W. E. Hendriksen, G. J. Koper, R. Eelkema and J. H. van Esch, *Science*, 2015, **349**, 1075–1079.
26 S. Maiti, I. Fortunati, C. Ferrante, P. Scrimin and L. J. Prins, *Nat. Chem.*, 2016, **8**, 725–731.
27 T. Heuser, A.-K. Steppert, C. Molano Lopez, B. Zhu and A. Walther, *Nano Lett.*, 2014, **15**, 2213–2219.

 This journal is © The Royal Society of Chemistry 2018

Published on 23 May 2018. Downloaded by Technical University of Munich on 14/06/2018 07:24:31.

28 J. Leira-Iglesias, A. Sorrenti, A. Sato, P. A. Dunne and T. M. Hermans, *Chem. Commun.*, 2016, **52**, 9009–9012.
29 A. Sorrenti, J. Leira-Iglesias, A. Sato and T. M. Hermans, *Nat. Commun.*, 2017, **8**, 15899.
30 F. J. Ndlec, T. Surrey, A. C. Maggs and S. Leibler, *Nature*, 1997, **389**, 305–308.
31 S. Roychowdhury and M. M. Rasenick, *Biochemistry*, 1994, **33**, 9800–9805.
32 L. S. Kariyawasam and C. S. Hartley, *J. Am. Chem. Soc.*, 2017, **139**, 11949–11955.
33 We can make this hypothesis because we find no delay between the kinetic of the chemical reaction network and the size or presence of the colloids. For example, the maximum size of the colloids is obtained at the same time as the maximum anhydride concentration, and the colloids disappear at exactly the moment the anhydride concentration falls below its solubility.
34 J. M. Neugebauer, *Methods Enzymol.*, 1990, **182**, 239–253.
35 P. Lo Nostro and B. W. Ninham, *Chem. Rev.*, 2012, **112**, 2286–2322.